How to cite: *Angew. Chem. Int. Ed.* **2020**, *59*, 14308–14312
International Edition: doi.org/10.1002/anie.202005047
German Edition: doi.org/10.1002/ange.202005047

Molecular Electronics

Understanding the Role of Parallel Pathways via In-Situ Switching of Quantum Interference in Molecular Tunneling Junctions

Saurabh Soni, Gang Ye, Jueting Zheng, Yanxi Zhang, Andika Asyuda, Michael Zharnikov, Wenjing Hong, and Ryan C. Chiechi**

Abstract: *This study describes the modulation of tunneling probabilities in molecular junctions by switching one of two parallel intramolecular pathways. A linearly conjugated molecular wire provides a rigid framework that allows a second, cross-conjugated pathway to be effectively switched on and off by protonation, affecting the total conductance of the junction. This approach works because a traversing electron interacts with the entire quantum-mechanical circuit simultaneously; Kirchhoff's rules do not apply. We confirm this concept by comparing the conductances of a series of compounds with single or parallel pathways in large-area junctions using EGaIn contacts and single-molecule break junctions using gold contacts. We affect switching selectively in one of two parallel pathways by converting a cross-conjugated carbonyl carbon into a trivalent carbocation, which replaces destructive quantum interference with a symmetrical resonance, causing an increase in transmission in the bias window.*

Research in molecular electronics (ME) is aimed at developing systems in which functionality is derived from the intrinsic molecular features. Molecular tunneling junctions exploit the quantum-mechanical nature of charge transport on the molecular scale, with the goal of developing devices with new logic and memory/storage processing systems at the molecular level.[1,2] Potentially useful elements of ME include switches,[3,4] quantum-interference-based molecular transistors,[5,6] rectifiers,[7–9] and thermoelectric molecular junctions.[10]

Destructive quantum interference (QI) is a particularly interesting phenomenon in the context of ME because it can lead to changes in conductance by orders of magnitude that can be manipulated via electrochemical gating, heteroatom substitution, change in bond topology, substitution effects, and other ways without altering the width of the tunneling barrier.[1,6,11–21] The relationship between bond topology, molecular orbitals and destructive QI features in transmission spectra is generally understood,[22] but theory overestimates the magnitudes of effects and is primarily useful for understanding trends in experimental data. Figure 1b schematically compares classical and quantum intramolecular circuits comprising two parallel pathways. In the former, the total conductance is the sum of individual contributions from individual pathways. In the latter, the individual pathways give rise to an extra quantum-mechanical term,[23] as each of them individually affect the electronic properties of junction due to QI.[24] Thus, a low-conductance cross-conjugated pathway in parallel with a high-conductance linear-conjugated pathway can suppress the overall transmission. Translating such phenomena into observable changes in tunneling is the first step towards realizing static devices. However, most QI studies involve single-molecule junctions, which are useful for fundamental studies but cannot be directly used in devices. In contrast, self-assembled monolayers (SAMs) are useful for fundamental studies and are capable of forming static devices, for example, proof-of-concept transistors based on gating QI features created by through-space intramolecular interactions.[5]

In our previous studies involving QI effects on linear-conjugated anthracene (AC) and cross-conjugated anthraquinone (AQ),[17,20] we showed that the tunneling current for AQ is suppressed because of the presence of destructive QI feature near the Fermi level (E_f) caused by the cross-conjugated bond topology. We further isolated the effects of bond topology by modifying the quinoid groups, finding that

[*] S. Soni, Dr. G. Ye,[++] Dr. Y. Zhang, Assoc. Prof. R. C. Chiechi
Stratingh Institute for Chemistry, University of Groningen
Nijenborgh 4, 9747 AG Groningen (The Netherlands)
E-mail: r.c.chiechi@rug.nl
S. Soni, Dr. G. Ye,[++] Dr. Y. Zhang, Assoc. Prof. R. C. Chiechi
Zernike Institute for Advanced Materials
Nijenborgh 4, 9747 AG Groningen (The Netherlands)
J. Zheng,[++] Prof. W. Hong
State Key Laboratory of Physical Chemistry of Solid Surfaces, College of Chemistry and Chemical Engineering, Xiamen University
Xiamen 361005 (China)
E-mail: whong@xmu.edu.cn
Dr. Y. Zhang
Present address: Microsystems, Department of Mechanical Engineering and Institute for Complex Molecular Systems, Eindhoven University of Technology
5600 MB Eindhoven (The Netherlands)
A. Asyuda, Prof. M. Zharnikov
Applied Physical Chemistry, Heidelberg University
Im Neuenheimer Feld 253, D-69120, Heidelberg (Germany)
Dr. G. Ye[++]
Center for Biomedical Optics and Photonics (CBOP) & College of Physics and Optoelectronic Engineering, Key Laboratory of Optoelectronic Devices and Systems, Shenzhen University
Shenzhen 518060 (P. R. China)
[++] equal second co-authorship.
Supporting information and the ORCID identification number(s) for the author(s) of this article can be found under: https://doi.org/10.1002/anie.202005047.

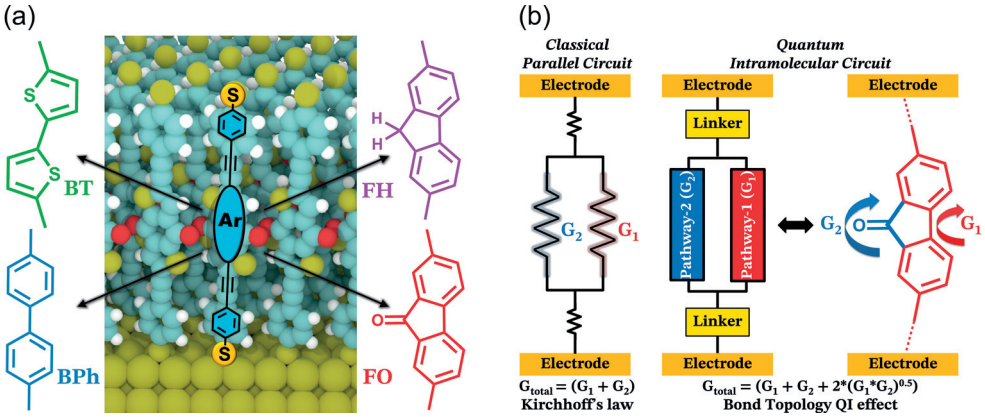

Figure 1. a) Self-assembled monolayers of molecular wires grown on Au^{TS} form static Au^{TS}/SAM//EGaIn junctions (/ and // denote covalent and van-der-Waals interfaces, respectively). The four cores corresponding to BT, BPh, FH, and FO. b) Classical resistors in parallel, based on the Kirchhoff's law compared to an intramolecular quantum circuit; for example, two parallel pathways in a tunneling junction in FO core, as indicated with the blue arrow for carbonyl and the red arrow for C–C single bond.

cross-conjugation leads to QI, but that specific functional groups can shift QI features in or out of the bias window.[16,25] Here, we exploit the quantum-mechanical nature of molecular circuits to eliminate QI features reversibly in situ via a cross-conjugated pathway that can be gated by protonation, but that is in parallel with a linear-conjugated pathway that provides structural rigidity. Gating occurs via the formation of trivalent carbon centers, which (like heteroatoms) are functionally linearly-conjugated.[26,27]

To isolate the effects of the two pathways and control differences that arise between single-molecule and SAM-based junctions, we studied four molecular wires shown in Figure 1a, that is, BT (bithiophene), BPh (biphenyl), FH (fluorene), and FO (fluorenone), along with AQ as a reference.[16] The aromatic cores of these molecules, decorated with thiol anchoring groups, were varied in the series to modify bond topology. Both BT and BPh are linearly conjugated; FH comprises parallel linear- and non-conjugated pathways; and FO comprises parallel linear- and cross-conjugated pathways. We characterized tunneling charge-transport in large-area junctions with an EGaIn top-contact and in single-molecule break junctions employing a scanning tunneling microscopy setup (STM-BJ). We support the experimental results with density functional theory (DFT) via non-equilibrium Green's function (NEGF) simulations that examine the role of trivalent carbon atoms in defining bond topology in the context of QI.

In our previous studies, simulations on single-molecule model junctions have agreed well with experimental results from large-area junctions exhibiting bond-topology based QI,[16,25,28] transition voltages,[16] molecular switches in SAMs,[4] and the mechanical and electrical stability of SAMs.[29] In this study, we used the model junction shown in Figure 2a, which comprises a finite central molecule between semi-infinite, periodic bulk electrodes.

Figure 2b shows the transmission probability vs. the electron energy, referenced to E_f. The respective transmission spectra show sharp dips (signature of destructive QI) and give zero-bias conductance values (G) as $G = G_0 \times T(E_f)$, where G_0 is the quantum of conductance ($G_0 = 2e^2/h = 77.48\ \mu S$) and $T(E_f)$ is the transmission probability at E_f. The results, which are summarized in Table 1, reveal five key features: 1) Linearly conjugated, planar BT has the second smallest optical band gap (E_g) and the highest zero-bias conductance; 2) Planar FH, with a linear- and a non-conjugated pathway in parallel, is the second-highest in conductance; 3) Linearly conjugated, twisted BPh (torsional angle = 40.3°) is less conductive than FH (in agreement with Venkataraman et al.[30]), but when constrained in planar conformation (as happens in SAMs[31,32]), the conductance of planar BPh overtakes FH, as shown in Figure S28; 4) Planar FO with a linear- and a cross-conjugated pathway in parallel has a destructive QI feature around $E - E_f = 1.5$ eV and is the least conductive, despite having the smallest E_g (Table 1); 5) For FOH (the protonated form of FO), the destructive QI feature

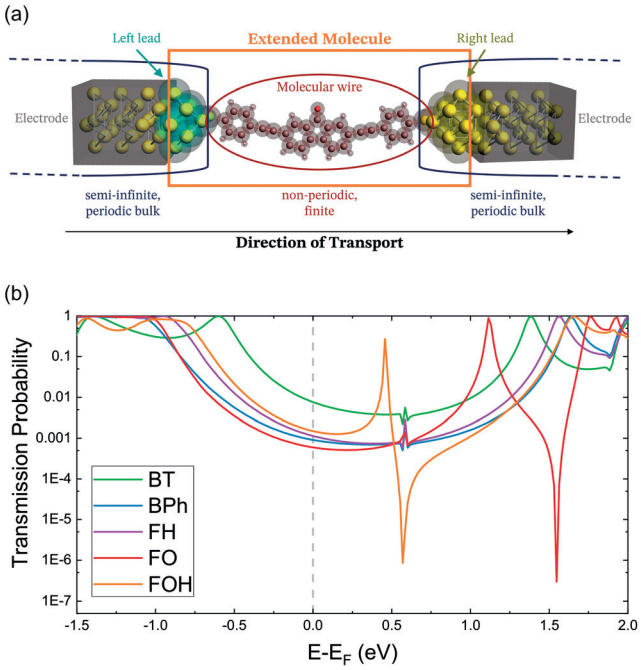

Figure 2. a) Simulated model junctions comprising an extended molecule (molecular wire connecting two leads made of the same material as the electrode) between semi-infinite periodic electrodes. b) Transmission probability vs. electron energy with respect to E_f for four molecular wires and FOH (protonated FO). As can be seen near E_f, the transmission trend is BT > FOH > FH > BPh > FO. The discontinuities in the transmission spectra at $E - E_f = 0.55$ eV are related to the effects of the potential in the contacts, see the Supporting Information for more details.

Table 1: Summary of the physical properties of BT, BPh, FH, FO, and FOH. Packing density is in the order of 10^{14} molecules cm^{-2}.

Compound	BT	BPh	FH	FO	FOH
UV/Vis E_g^{opt} (eV)	2.73	3.27	3.19	2.45	2.17
EGaIn low-bias G (10^{-3} S cm^{-2})	28.2 ± 0.43	16.1 ± 0.36	11.38 ± 0.17	4.15 ± 0.06	–
STM-BJ G ($\log(G/G_0)$)	−3.92 ± 0.04	−4.35 ± 0.03	−4.16 ± 0.05	−4.26 ± 0.07	−3.89 ± 0.07
DFT G ($\log(G/G_0)$)	−2.11	−3.04 (−2.70[a])	−2.94	−3.22	−2.81
XPS thickness (Å)	18.3 ± 1	20.5 ± 1	20.4 ± 1	18.2 ± 1	–
Packing density	5.5 ± 0.55	3.0 ± 0.3	2.6 ± 0.26	5.1 ± 0.51	–
Yield of EGaIn junctions	80.0%	78.9%	82.4%	85.7%	–

[a] for the planar BPh structure.

near 1.5 eV disappears and a symmetrical feature appears near 0.5 eV, leading to an increase in transmission at E_f. Simulations on FOH in the presence of TFA^- anions are shown in the Supporting Information.

We investigated the tunneling transport of the four molecules in large-area Au^{TS}/SAM//EGaIn junctions (where / and // denote a covalent and van-der-Waals interface, respectively, and Au^{TS} is an ultraflat template-stripped Au substrate). The Supporting Information details the SAM-formation procedure and characterization via the water contact angle, and synchrotron-based X-ray photoelectron spectroscopy (XPS), the results of which are summarized in Table 1. As shown in Figure 3 (black dashed line), the order of current density in large-area junctions is BT ≥ BPh > FH > FO (full-scale J–V curves are shown in the Supporting Information). The observation that BPh is more conductive than FH reflects the participation of the non-conjugated pathway in FH; The linearly conjugated pathways in BPh and FH are identical because BPh is planarized in the SAMs, but tunneling electrons simultaneously sample that pathway and the methylene bridge of FH because it is part of the σ-bond framework. Replacing the methylene bridge with a carbonyl group converts non-conjugation into cross-conjugation, thus FO is even less conductive than FH. This counter-intuitive result is, again, a reflection of the nature of quantum mechanical circuits; cross-conjugation leads to destructive QI, which suppresses conductance more than non-conjugation. The trends in low-bias EGaIn conductance and zero-bias DFT conductance (black and blue dashed lines, respectively, in Figure 3) are in good agreement, suggesting that our simulated model junction captures the properties of large-area junctions, provided the correct molecular geometries are used.

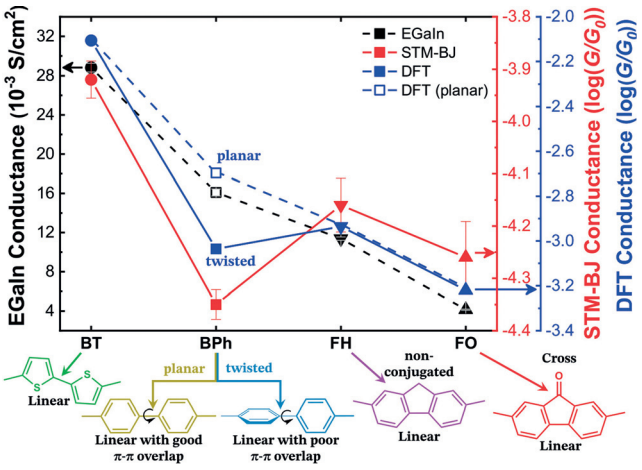

Figure 3. Experimental and simulated conductance data for BT (●), BPh planar (□), BPh (twisted, ■), FH (▼), and FO (▲). Here, we compare the low-bias EGaIn conductance (black dashed line, left axis), zero-bias STM-BJ conductance (red solid line, red axis on the right), and zero-bias DFT conductance (blue dashed and solid lines, blue axis on the right). The DFT data connected by dashed blue and solid blue lines are the simulations of EGaIn and STM-BJ data, respectively. The molecular structures with type of conjugation are shown at the bottom. For sake of clarity, pathways in FH and FO are labeled as non-conjugated and linearly conjugated as well as cross-conjugated and linearly conjugated, respectively.

To exclude the possibility that intermolecular pathways play a significant role, we performed single-molecule conductance measurements in the STM-BJ setup (see the Supporting Information for details). As shown in Figure 3, the conductance trend follows BT > FH ≥ FO > BPh (solid red line), in agreement with DFT simulations (solid blue line). The trend in single-molecule conductance also agrees with EGaIn results except that, as expected, BPh is much less conductive because it can adopt its preferred, twisted geometry in solution. This discrepancy further supports our assertion that, in large-area junctions, conductance is dominated by transport through individual molecules and that the only significant experimental variable is the conformation that the molecules adopt in the two different measurement platforms.[28]

Protonation of FO is predicted to increase transmission. The increase in transmission probability near E_f in Figure 2b is modest, but is accompanied by the loss of a destructive QI feature and the appearance of a symmetric feature near 0.5 eV. This feature resembles a Fano resonance, implying that the trivalent carbon in FOH remains strongly coupled to the linearly conjugated pathway, but is itself weakly coupled to the electrodes.[14] While the entire transmission spectrum contributes to the overall tunneling probability, empirically, the observed conductance is dominated by transmission near E_f.[16]

To test for the predicted increase in conductance upon protonation, we measured FO in single-molecule junctions in the presence and absence of trifluoroacetic acid (TFA), using FH as a control. Although FO is a weak base, in the presence of TFA there will be a small concentration of FOH present at equilibrium. If FOH is more conductive than FO, it should shift the peak of the conductance histogram by a degree commensurate with the equilibrium concentration and the difference in conductance between FO and FOH.

We prepared solutions of FO and FH with same concentrations as before, adding 30% (v/v) TFA to effect protonation. As can be seen from Figure 4a, while the conductance

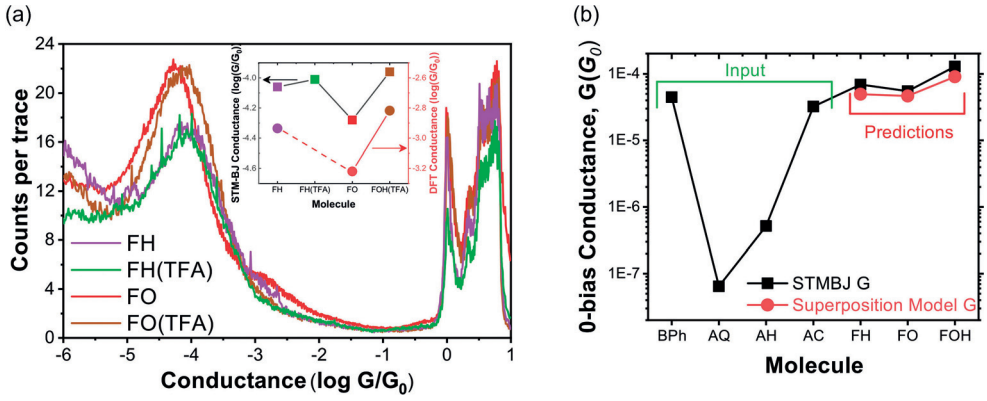

Figure 4. a) Histograms of counts vs. conductance from STM-BJ measurements on FO and FH with and without treatment with TFA. FH remains unaffected, however, the conductance of FO increases upon protonation. Inset: Mean STM-BJ conductance (left axis) and DFT-predicted conductance trend (right axis). b) STM-BJ conductance of the seven molecules (black squares) and predicted conductances of FH, FO, and FOH (red circles), see the Supporting Infomration for further details.

histogram of FH + TFA does not differ from that of FH, that of FO + TFA is shifted to higher conductances. In our previous work on the inclusion of trivalent carbon centers in conjugated materials, they were functionally linearly conjugated through an empty p-orbital.[26,27] The trend in conductance in the inset of Figure 4a suggests the same in single-molecule junctions and validates the DFT-NEGF prediction of FOH > FH > FO.

Supported by experiments involving large-area and single-molecule junctions, DFT-NEGF and an empirical superposition model (see Figure 4b and the Supporting Information), we show that tunneling charge transport across a molecular framework can be manipulated by altering conjugated pathways in parallel with linearly conjugated pathways. Although we have not yet succeeded in switching the test molecular wire, FO, in SAMs, we are pursuing systems that are more readily protonated for this purpose. Nonetheless, the parallel-pathway approach to switching allows the in-place manipulation of QI-controlling bond topology without large structural changes, making it a viable strategy for QI switching in static, large-area molecular tunneling junctions.

Acknowledgements

R.C.C. and Y.Z. acknowledge the European Research Council for the ERC Starting Grant 335473 (MOLECSYNCON). S.S. acknowledges the Zernike Institute for Advanced Materials. G.Y. acknowledges financial support from the China Scholarship Council (CSC):NO.201408440247. We thank the Center for Information Technology of the University of Groningen for their support and for providing access to the Peregrine high performance computing cluster. A.A. and M.Z thank the Helmholtz Zentrum Berlin for the allocation of synchrotron radiation beamtime at BESSY II and financial support as well as A. Nefedov and Ch. Wöll for the technical cooperation during the experiments at BESSY II. We thank E. Sauter for participation in some of the experiments in context of this project. A.A. acknowledges the financial support by the DAAD-ACEH Scholarship of Excellence. W.H. and J.Z. acknowledge the financial support from the National Natural Science Foundation of China (No. 21673195) and the National Key R&D Program of China (2017YFA0204902). We thank Dr. Remco W. A. Havenith for insightful discussion and help with the ADF theoretical simulations and NWO for access to the Dutch national e-infrastructure. Part of this work was carried out on the Dutch national e-infrastructure (Cartesius) with the support of SURF Cooperative.

Conflict of interest

The authors declare no conflict of interest.

Keywords: EGaIn · molecular electronics · quantum interference · self-assembled monolayers · STM-BJ

[1] M. Lörtscher, *Chem* **2017**, *3*, 376–377.
[2] J. C. Love, L. a. Estroff, J. K. Kriebel, R. G. Nuzzo, G. M. Whitesides, *Chem. Rev.* **2005**, *105*, 1103–1170.
[3] X. Huang, T. Li, *J. Mater. Chem. C* **2020**, *8*, 821–848.
[4] S. Kumar, J. T. van Herpt, R. Y. N. Gengler, B. L. Feringa, P. Rudolf, R. C. Chiechi, *J. Am. Chem. Soc.* **2016**, *138*, 12519–12526.
[5] C. Jia, M. Famili, M. Carlotti, Y. Liu, P. Wang, I. M. Grace, Z. Feng, Y. Wang, Z. Zhao, M. Ding, X. Xu, C. Wang, S.-J. Lee, Y. Huang, R. C. Chiechi, C. J. Lambert, X. Duan, *Sci. Adv.* **2018**, *4*, eaat8237.
[6] M. Koole, J. M. Thijssen, H. Valkenier, J. C. Hummelen, H. S. J. van der Zant, *Nano Lett.* **2015**, *15*, 5569–5573.
[7] L. Qiu, Y. Zhang, T. L. Krijger, X. Qiu, P. v. Hof, J. C. Hummelen, R. C. Chiechi, *Chem. Sci.* **2017**, *8*, 2365–2372.
[8] N. Nerngchamnong, L. Yuan, D.-C. Qi, J. Li, D. Thompson, C. a. Nijhuis, *Nat. Nanotechnol.* **2013**, *8*, 113–118.
[9] X. Chen, M. Roemer, L. Yuan, W. Du, D. Thompson, E. del Barco, C. A. Nijhuis, *Nat. Nanotechnol.* **2017**, *12*, 797.
[10] D. Z. Manrique, Q. Al-Galiby, W. Hong, C. J. Lambert, *Nano Lett.* **2016**, *16*, 1308–1316.
[11] Y. Zhang, Z. Zhao, D. Fracasso, R. C. Chiechi, *Isr. J. Chem.* **2014**, *54*, 513–533.
[12] N. Xin, X. Guo, *Chem* **2017**, *3*, 373–376.
[13] G. C. Solomon, D. Q. Andrews, R. H. Goldsmith, T. Hansen, M. R. Wasielewski, R. P. Van Duyne, M. a. Ratner, *J. Am. Chem. Soc.* **2008**, *130*, 17301–17308.
[14] C. J. Lambert, *Chem. Soc. Rev.* **2015**, *44*, 875–888.
[15] G. C. Solomon, C. Herrmann, T. Hansen, V. Mujica, M. A. Ratner, *Nat. Chem.* **2010**, *2*, 223–228.
[16] Y. Zhang, G. Ye, S. Soni, X. Qiu, T. L. Krijger, H. T. Jonkman, M. Carlotti, E. Sauter, M. Zharnikov, R. C. Chiechi, *Chem. Sci.* **2018**, *9*, 4414–4423.
[17] D. Fracasso, H. Valkenier, J. C. Hummelen, G. C. Solomon, R. C. Chiechi, *J. Am. Chem. Soc.* **2011**, *133*, 9556–9563.

[18] D. Q. Andrews, G. C. Solomon, R. H. Goldsmith, T. Hansen, M. R. Wasielewski, R. P. V. Duyne, M. A. Ratner, *J. Phys. Chem. C* **2008**, *112*, 16991 – 16998.
[19] C. R. Arroyo, S. Tarkuc, R. Frisenda, J. S. Seldenthuis, C. H. M. Woerde, R. Eelkema, F. C. Grozema, H. S. J. van der Zant, *Angew. Chem. Int. Ed.* **2013**, *52*, 3152 – 3155; *Angew. Chem.* **2013**, *125*, 3234 – 3237.
[20] H. Valkenier, C. M. Guedon, T. Markussen, K. S. Thygesen, S. J. van der Molen, J. C. Hummelen, *Phys. Chem. Chem. Phys.* **2014**, *16*, 653 – 662.
[21] X. Liu, S. Sangtarash, D. Reber, D. Zhang, H. Sadeghi, J. Shi, Z.-Y. Xiao, W. Hong, C. J. Lambert, S.-X. Liu, *Angew. Chem. Int. Ed.* **2017**, *56*, 173 – 176; *Angew. Chem.* **2017**, *129*, 179 – 182.
[22] T. Markussen, R. Stadler, K. S. Thygesen, *Nano Lett.* **2010**, *10*, 4260 – 4265.
[23] M. Magoga, C. Joachim, *Phys. Rev. B* **1999**, *59*, 16011 – 16021.
[24] H. Chen, H. Zheng, C. Hu, K. Cai, Y. Jiao, L. Zhang, F. Jiang, I. Roy, Y. Qiu, D. Shen, Y. Feng, F. M. Alsubaie, H. Guo, W. Hong, J. F. Stoddart, *Matter* **2020**, *2*, 378 – 389.
[25] M. Carlotti, S. Soni, X. Qiu, E. Sauter, M. Zharnikov, R. C. Chiechi, *Nanoscale Adv.* **2019**, *1*, 2018 – 2028.
[26] T. P. Voortman, R. C. Chiechi, *ACS Appl. Mater. Interfaces* **2015**, *7*, 28006 – 28012.
[27] G. Ye, N. Y. Doumon, S. Rousseva, Y. Liu, M. Abdu-Aguye, M. A. Loi, J. C. Hummelen, L. J. A. Koster, R. C. Chiechi, *ACS Appl. Energy Mater.* **2019**, *2*, 2197 – 2204.
[28] M. Carlotti, A. Kovalchuk, T. Wächter, X. Qiu, M. Zharnikov, R. C. Chiechi, *Nat. Commun.* **2016**, *7*, 13904.
[29] Y. Zhang, X. Qiu, P. Gordiichuk, S. Soni, T. L. Krijger, A. Herrmann, R. C. Chiechi, *J. Phys. Chem. C* **2017**, *121*, 14920 – 14928.
[30] L. Venkataraman, J. E. Klare, C. Nuckolls, M. S. Hybertsen, M. L. Steigerwald, *Nature* **2006**, *442*, 904 – 907.
[31] J. Trotter, *Acta Crystallogr.* **1961**, *14*, 1135 – 1140.
[32] A. Shaporenko, M. Elbing, A. Błaszczyk, C. Von Hänisch, M. Mayor, M. Zharnikov, *J. Phys. Chem. B* **2006**, *110*, 4307 – 4317.

Manuscript received: April 7, 2020
Accepted manuscript online: May 29, 2020
Version of record online: July 3, 2020

